

THE DEEP2 GALAXY REDSHIFT SURVEY: THE EVOLUTION OF VOID STATISTICS FROM $Z \sim 1$ TO $Z \sim 0$

CHARLIE CONROY¹, ALISON L. COIL¹, MARTIN WHITE^{1,3}, JEFFREY A. NEWMAN², RENBIN YAN¹, MICHAEL C. COOPER¹,
BRIAN F. GERKE³, MARC DAVIS^{1,3}, DAVID C. KOO⁴

Draft version July 16, 2021

ABSTRACT

We present measurements of the void probability function (VPF) at $z \sim 1$ using data from the DEEP2 Redshift Survey and its evolution to $z \sim 0$ using data from the Sloan Digital Sky Survey (SDSS). We measure the VPF as a function of galaxy color and luminosity in both surveys and find that it mimics trends displayed in the two-point correlation function, ξ ; namely that samples of brighter, red galaxies have larger voids (i.e. are more strongly clustered) than fainter, blue galaxies. We also clearly detect evolution in the VPF with cosmic time, with voids being larger in comoving units at $z \sim 0$. We find that the reduced VPF matches the predictions of a ‘negative binomial’ model for galaxies of all colors, luminosities, and redshifts studied. This model lacks a physical motivation, but produces a simple analytic prediction for sources of any number density and integrated two-point correlation function, $\bar{\xi}$. This implies that differences in the VPF across different galaxy populations are consistent with being due entirely to differences in the population number density and $\bar{\xi}$. We compare the VPF at $z \sim 1$ to N -body Λ CDM simulations and find good agreement between the DEEP2 data and mock galaxy catalogs. Interestingly, we find that the dark matter *particle* reduced VPF follows the physically motivated ‘thermodynamic’ model, while the dark matter *halo* reduced VPF more closely follows the negative binomial model. The robust result that all galaxy populations follow the negative binomial model appears to be due to primarily to the clustering of dark matter halos. The reduced VPF is insensitive to changes in the parameters of the halo occupation distribution, in the sense that halo models with the same $\bar{\xi}$ will produce the same VPF. For the wide range of galaxies studied, the VPF therefore does not appear to provide useful constraints on galaxy evolution models that cannot be gleaned from studies of $\bar{\xi}$ alone.

Subject headings: galaxies: evolution — galaxies: dark matter — galaxies: clustering

1. INTRODUCTION

Voids are some of the most striking large-scale features of the Universe. Historically, their study can be loosely grouped into two categories: finding individual voids or using a statistical approach (see Rood (1988) for a detailed review of the history of void studies). The first focuses on identifying individual voids with sophisticated void-finding algorithms (Kauffmann & Fairall 1991; Kauffmann & Melott 1992; El-Ad, Piran, & da Costa 1996; Ryden & Melott 1996; El-Ad & Piran 1997; Aikio & Maehoenen 1998; Sheth et al. 2003; Patiri et al. 2005) that allow voids to have any convex shape. The properties of galaxies in voids can then be studied, including their color distribution, luminosity function, concentrations and star-formation rates (Grogin & Geller 1999, 2000; Rojas et al. 2004; Hoyle et al. 2005; Rojas et al. 2005). Hoyle & Vogeley (2004) analyze the recently-completed 2dF Galaxy Redshift Survey and find that void galaxies are, on average, bluer and show evidence for more recent star-formation than the full 2dF galaxy population. Properties of voids themselves can also be studied,

including characteristic sizes, mean ellipticities, and radial density profiles. Many of these observational quantities, such as size measurements, can only be interpreted with carefully constructed mock galaxy catalogs. Extensive theoretical work has been carried out concerning void size distributions and density profiles (Sheth & van de Weygaert 2004; Benson et al. 2003; Colberg et al. 2005; Shandarin, Sheth, & Sahni 2004; Patiri et al. 2004), void halo properties (Antonuccio-Delogu et al. 2002; Gottlöber et al. 2003; Goldberg & Vogeley 2004; Patiri et al. 2004; Colberg et al. 2005), formation of galaxies within voids (Mathis & White 2002), and the properties of galaxies in voids (Benson et al. 2003). The question of whether simulations can produce voids as large and as empty as voids seen in the observed Universe remains unanswered, and can potentially provide powerful constraints on galaxy formation and cosmology (Peebles 2001).

The second approach to voids is somewhat more statistical and is in many ways complementary to the first. Studies of this type focus primarily on the void probability function (VPF) which is defined as the probability that a sphere of a given size centered on a random point in the survey volume contains no galaxies. Statistical void distributions in principle offer a wealth of information, as they can be related to the entire hierarchy of galaxy correlation functions (White 1979). Yet, due to the difficulties in interpreting void statistics, they have not received as much attention as more conventional statistical measures of large-scale structure such as the two-point correlation function.

¹ Department of Astronomy, University of California, Berkeley, CA 94720 – 3411

² Hubble Fellow, Lawrence Berkeley National Laboratory, 1 Cyclotron Road, Berkeley, CA 94720

³ Department of Physics, University of California, Berkeley, CA 94720 – 3411

⁴ University of California Observatories/Lick Observatory, Department of Astronomy and Astrophysics, University of California, Santa Cruz, CA 95064

Despite these difficulties, the theoretical framework underlying void statistics has been developed in detail (White 1979; Fry 1984, 1985, 1986; Otto et al. 1986; Fry 1988; Sheth 1996; Balian & Schaeffer 1989), and has been extensively studied in simulations (e.g. Fry et al. 1989; Ghigna et al. 1994, 1996; Ryden & Melott 1996; Kauffmann, Nusser, & Steinmetz 1997; Schmidt, Ryden, & Melott 2001; Berlind & Weinberg 2002; Benson et al. 2003).

Observationally, voids statistics have been investigated in almost every major galaxy redshift survey, including the CfA (Maurogordato & Lachize-Rey 1987; Vogeley, Geller, & Huchra 1991; Vogeley et al. 1994; Mo & Boerner 1990), SSRS (Gaztanaga & Yokoyama 1993), PSCz (Hoyle & Vogeley 2002), IRAS (El-Ad, Piran, & Dacosta 1997), LCRS (Müller et al. 2000) and most recently, the 2dF survey (Hoyle & Vogeley 2004; Croton et al. 2004; Patiri et al. 2005). Results from the latter survey are representative of an emerging consensus; subsamples of brighter and/or redder galaxies contain larger voids than samples of fainter and/or bluer galaxies. This is interpreted as brighter and/or redder populations being more strongly clustered than fainter and/or bluer subsamples. These trends are also reflected in the two-point correlation function of galaxies, ξ , both at low (e.g., Zehavi et al. 2002) and moderate (e.g., Coil et al. 2004b) redshifts. We note that some studies of voids have not taken into account the fact that galaxy populations have different number densities which will strongly affect void statistics; hence differences in the VPF across galaxy populations might as easily be attributable to the luminosity function as to varying clustering strengths. As brighter galaxies are rarer than fainter galaxies, even in volume-limited samples, brighter samples will have higher void probabilities. A critical question we wish to address here is the extent to which void statistics are governed by low-order clustering statistics. It is therefore important to separate the effects of clustering from the effects of number density on the VPF.

Void statistics can also be used to probe the relation between galaxies and dark matter. There are strong theoretical arguments that show that the clustering strength of dark matter and galaxies should be different (e.g., Kaiser 1984; Bardeen et al. 1986; Efstathiou et al. 1988; Cole & Kaiser 1989; Mo & White 1996). Galaxies initially form in high density peaks of the dark matter distribution and hence are “biased” tracers of the dark matter at high redshift. Baryonic physics and cosmic evolution also lead one to expect that the biasing between galaxies and dark matter should, in principle, be a function of scale, redshift, and galaxy properties such as color and luminosity. Many of these expectations have been borne out in observations (see for example Davis & Geller 1976; Loveday et al. 1995; Zehavi et al. 2002; Madgwick et al. 2003; Coil et al. 2004b).

By studying voids in observational samples and comparing to dark matter simulations, one can hope to probe the galaxy bias in a unique way. The VPF has previously been studied in simulations where a biasing prescription was assumed in order to place galaxies in the dark matter distribution (e.g., Little & Weinberg 1994; Kauffmann, Nusser, & Steinmetz 1997; Berlind & Weinberg 2002; Ghigna et al. 1994, 1996).

Kauffmann, Nusser, & Steinmetz (1997) find that the VPF has limited utility in probing the bias, as the relation between dark matter and galaxies changes as a function of the sampling density of a galaxy survey. Weinberg & Cole (1992) and Little & Weinberg (1994) however, find that the VPF can be a powerful discriminator between various biasing schemes, but that it is relatively insensitive to the value of the linear bias factor $b \equiv (\xi_{gal}/\xi_{dm})^{1/2}$. For example, the VPF is very different, for fixed b , when one statistically identifies galaxies with overdensities in the initial density field (‘peaks biasing’) versus identifying galaxies with overdensities in the final matter distribution (‘density biasing’).

More recently, the halo model (e.g., Seljak 2000; Peacock & Smith 2000; Cooray & Sheth 2002; Kravtsov et al. 2004) has emerged as a useful prescription for placing galaxies within dark matter simulations. Instead of using a biasing scheme such as ‘peaks biasing’ or ‘density biasing’ to relate galaxies to the dark matter distribution, the halo model places galaxies within virialized dark matter halos as a function of the halo mass. Although in principle the parameters of the halo model can evolve with cosmic time, there is evidence to suggest that the model does not strongly evolve from $z \sim 1$ to $z \sim 0$ (Yan, Madgwick, & White 2003). Berlind & Weinberg (2002) find that the VPF can be used to determine halo model parameters such as the minimum dark matter halo mass, M_{min} , in which a galaxy of a given luminosity may exist, and can hence provide useful new constraints on the relation between galaxies and dark matter. In this paper we explore in detail the possibility of using the VPF to constrain the halo model.

Until now, there has not been sufficient data to study the statistics of voids at intermediate redshift ($z > 0.3$). From correlation function measurements using the DEEP2 dataset at $z \sim 1$ (Coil et al. 2004b) we know that galaxies were in general less strongly clustered in the past; one might expect this trend to be reflected in void statistics as well. As more data becomes available at higher redshifts, the importance of self-consistently investigating the evolution of galaxy properties and statistics cannot be overemphasized. This entails using similar selection and analysis techniques at different redshifts. For this reason, we have chosen to include in this study an analysis of the SDSS, which now has data for $\sim 200,000$ galaxies at $z < 0.2$, to allow for robust conclusions concerning the evolution of void statistics.

It should be kept in mind that the two approaches to the study of voids outlined above use the term “void” in very different ways. While the first approach identifies voids as large underdensities in the galaxy distribution, allowing a void to assume any convex shape and allowing galaxies to exist inside voids, the second approach identifies voids as spherical regions in which surveyed galaxies are totally absent. Furthermore, while the first approach only locates “unique” voids, insofar as it does not allow smaller “sub-voids” to be contained within larger voids, the second approach allows for “voids” to overlap (see §5 for a visualization of this idea). The statistical approach is only interested in the question: what is the probability that a given volume element in the universe is empty? In this paper we are concerned with the second, statistical

approach, and hence we define voids in the latter sense.

The rest of this paper is organized as follows. In §2 we outline the theory behind void statistics and point out several problems that arise with the theoretical underpinnings of voids. §3 describes our methodology. We statistically analyze voids in mock galaxy catalogs built from N-body simulations in §4; in §5 we present our results from the DEEP2 galaxy survey at $z \sim 1$ and in §6 we analyze the SDSS galaxy survey at $z \sim 0$. §7 discusses the implications and relevance of our results. Throughout this paper we assume a flat concordance Λ CDM cosmology with $\Omega_m = 0.3$, $\Omega_\Lambda = 1 - \Omega_m = 0.7$ and $H_0 = 100 h \text{ km s}^{-1} \text{ Mpc}^{-1}$.

2. THEORETICAL BACKGROUND

2.1. General Considerations

The void probability function (VPF) is defined as the probability of finding no galaxies inside a sphere of radius R , randomly placed within a sample. The most common theoretical interpretation of the VPF is as an infinite sum of the hierarchy of correlation functions of the galaxy distribution (White 1979; Sheth 1996). Specifically, for spherical volume elements one may write the VPF as:

$$P_0(R) = \exp \left[\sum_{p=1}^{\infty} \frac{-\bar{N}(R)^p}{p!} \bar{\xi}_p(R) \right], \quad (1)$$

where R is the sphere radius, \bar{N} is the average number of galaxies within the sphere, and $\bar{\xi}_p$ is the volume averaged p -point correlation function, where the volume average is defined by

$$\bar{\xi}_p \equiv \frac{\int \xi_p dV}{\int dV}. \quad (2)$$

As P_0 depends on a recurring factor of \bar{N} , any meaningful comparison of P_0 between populations requires a careful handling of their number densities. For many comparisons made in this study, we choose to remove the dependency on \bar{N} by randomly diluting the samples to have similar number densities. In this way we can isolate the effects of clustering on the VPF.

The VPF takes a much simpler form if one uses the hierarchical *Ansatz*,

$$\bar{\xi}_p = S_p \bar{\xi}^{p-1}, \quad p \geq 3 \quad (3)$$

to relate the hierarchy of correlation functions to the two-point function, $\bar{\xi}$. This allows for a complete and relatively simple description of the entire cosmological density field. The *Ansatz* has been formally derived only for an $\Omega_m = 1$ universe with the additional assumptions of stable clustering and self-similarity (Bernardeau et al. 2002), which are both known to be invalid. In the linear regime ($R \gtrsim 15 \text{ Mpc}$) perturbation theory seems to validate the *Ansatz*, although this paper is largely confined to smaller scales. So far, the *Ansatz* has not been ruled out by observations (see e.g. Gaztanaga 1992; Gaztanaga et al. 1995; Baugh et al. 2004), although it is worth mentioning that Baugh et al. had to remove the largest structure in their sample in order to recover scale invariant S_p values. There is no reason to believe that the *Ansatz* should hold in the quasi-linear to strongly nonlinear regimes. Although historically the S_p values

were assumed to be scale invariant, nothing in the formalism developed below requires them to be. With the hierarchical *Ansatz* the VPF becomes:

$$P_0 = \exp \left[\sum_{p=1}^{\infty} \frac{-\bar{N}^p}{p!} S_p \bar{\xi}^{p-1} \right]. \quad (4)$$

Fry (1986) noted that Eqn. 4 could be manipulated to isolate the effects of the scaling coefficients (S_p). Fry defined the reduced void probability function, χ :

$$\chi \equiv -\ln(P_0)/\bar{N} \quad (5)$$

which, with the substitution of Eqn. 4 becomes:

$$\chi(\bar{N}\bar{\xi}) = \sum_{p=1}^{\infty} \frac{S_p}{p!} (-\bar{N}\bar{\xi})^{p-1}. \quad (6)$$

With this definition, $\bar{N}\bar{\xi}$ becomes the independent variable, and hence only populations of galaxies with different S_p values will have different reduced VPFs. Although $\bar{N}\bar{\xi}$ will in general have a different dependence on R for each galaxy population, this quantity will always be an increasing function of R since $\bar{N} \propto R^3$ and $\bar{\xi} \propto R^{-\gamma}$ with $\gamma < 3$ for all of the populations considered here. We now briefly summarize several models which predict values for the S_p values.

2.2. Hierarchical Models

As the dynamical equations governing gravitational clustering can not be solved in the weakly to strongly nonlinear regime using perturbation theory (or any of its offspring), various phenomenological models have been proposed to relate the higher order correlation functions to the two-point correlation function. These models provide a complete description of gravitational clustering, yet each is inadequate either theoretically or observationally. See Fig. 1 for examples of predictions of the VPF from some of the more popular models; for a detailed treatment see Fry (1986, 1988).

In a Poisson model, all moments with $p > 1$ vanish, and the VPF can be described simply by:

$$P_0 = e^{-\bar{N}}, \quad \chi = 1. \quad (7)$$

A Gaussian model is almost as simple and equally inapplicable to the statistics of large scale structure in the universe on nonlinear scales at late times. This model implies that the entire statistical distribution is described by the two-point moment (in this case $\bar{\xi}$) and that all higher moments identically vanish. The Gaussian and Poisson models are obviously not actually hierarchical models; we include them under 'hierarchical models' for simplicity.

More realistic models rely on the hierarchical *Ansatz* to specify all possible moments of the galaxy distribution. These models can be thought of as prescriptions for the S_p scaling coefficients. The simplest model in this case forces $S_p = 1$ for all p and is sensibly called the 'Minimal' model (Fry 1986). Yet another model was motivated by an attempt to combine the hierarchical *Ansatz* with the BBGKY kinetic equations (Fry 1984). The BBGKY model becomes unphysical for large void radii, as can be seen in Fig. 1 where χ becomes negative for $\bar{N}\bar{\xi} > 30$.

The 'thermodynamic model' was first proposed by Saslaw & Hamilton (1984) and arose from a theory which

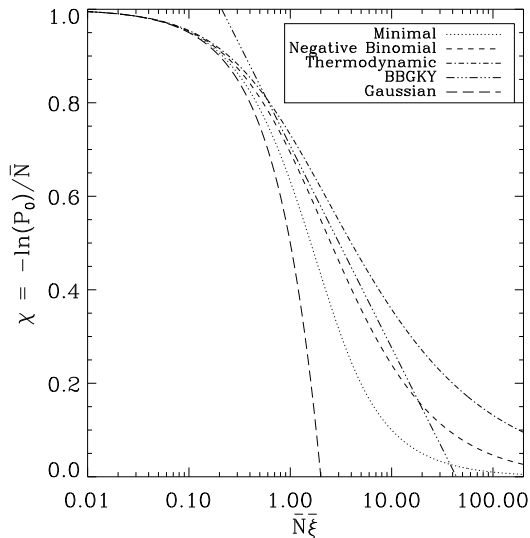


FIG. 1.— Reduced VPF for several of the hierarchical models discussed in §2. The models are most easily distinguished from one another for $\bar{N}\bar{\xi} > 5$, a region that can be investigated with currently existing low- and high-redshift galaxy samples. Note that the Poisson model requires $\chi = 1$.

treated galaxy clustering by analogy to statistical mechanics. It was later extended into a more self-consistent model by Fry (1986):

$$\chi = [(1 + 2\bar{N}\bar{\xi})^{1/2} - 1]/\bar{N}\bar{\xi}, \quad (8)$$

$$S_p = (2p - 3)!! \quad (9)$$

Intriguingly, a model developed by Sheth (1998) which combines an excursion set approach to the evolution of the halo mass function with a simple model for the spatial distribution of such halos predicts the same values for S_p . Fry (1985) points out that this theory is only strictly true for large volumes, and that the derivations do not apply for $\xi \sim 1$ ($r \sim 5 h^{-1}$ Mpc). It is also difficult to understand how such large scales could have become thermodynamically relaxed over the age of the universe. Hamilton et al. (1985) compared this model prediction to the VPF from the CfA survey, but their results were inconclusive. They did find, however, that volume limited subsamples of different minimum luminosities were hierarchically related in that samples with different \bar{N} and $\bar{\xi}$, had similar S_p .

The final model we consider has had a colorful history. The negative binomial distribution, also known as the modified Bose-Einstein distribution, was used early on by Carruthers & Shih (1983) to study the count distribution of charged hadrons resulting from high-energy collisions and by Carruthers & Duong-van (1983) to describe the observed distribution of Zwicky clusters. The model can be described by:

$$\chi = \ln(1 + \bar{N}\bar{\xi})/\bar{N}\bar{\xi}, \quad (10)$$

$$S_p = (p - 1)!, \quad (11)$$

$$P_0 = \left[\frac{1}{1 + \bar{N}\bar{\xi}} \right]^{1/\bar{\xi}}. \quad (12)$$

Gaztanaga & Yokoyama (1993) analyzed the reduced VPF in the SSRS2 and CfA redshift surveys but could

not discriminate between the thermodynamic and negative binomial models because of the size of their errors. The negative binomial distribution was re-derived in their appendix by considering a sample divided into small cells, with the occupation probability of each cell depending only on $\bar{\xi}$, and being independent of the other cells (see also Elizalde & Gaztanaga 1992). Unfortunately, the derivation contains little insight into the physical mechanisms that might drive point distributions to become negative binomial. This model has also been derived from thermodynamic arguments (Sheth 1995).

Mo & Boerner (1990) and Vogeley, Geller, & Huchra (1991) independently analyzed the CfA survey and found the data to be more consistent with the negative binomial than thermodynamic model over a range of luminosity thresholds and morphological types, though the agreement between model and data was not conclusive. Most recently, Croton et al. (2004) found that galaxies in the 2dF survey follow the negative binomial model over a range of differential luminosity bins.

2.3. Convergence Issues

The astute reader will have noticed two problems with the theoretical models presented above, one related to convergence and the other to the unintuitive nature of the sums in Eqns. 1, 4 and 6. The form for the S_p values associated with the thermodynamic and negative binomial models (Eqns. 9 and 11) can be understood as arising from a Taylor series expansion for the given χ values in Eqns. 8 and 10. Such an expansion is, however, only valid for $\bar{N}\bar{\xi} < 1$; the sum rapidly diverges if $\bar{N}\bar{\xi} > 1$. The conclusion must be that the S_p values often quoted for these models cannot be correct for large $\bar{N}\bar{\xi}$, i.e. for $r \gtrsim 3 h^{-1}$ Mpc (the precise r at which $\bar{N}\bar{\xi} = 1$ depends on the sample).

Realizing this issue, we have explored other forms for the S_p values such that the sums in Eqns. 4 and 6 do converge. Simplistic models such as:

$$S_p = e^{Ap+B}, \quad (13)$$

where A and B are free parameters, are consistent with recent observations of S_p for $p < 6$ (Baugh et al. 2004) and are also consistent with $(p - 1)!$ for small p . Although the sums converge with these S_p values, they do not converge to a hierarchical model; in fact, for many values of A and B, the sums converge to non-physical values ($P_0 < 0$). It is unclear how far one should pursue this, given (1) that the S_p values are probably scale-dependent, and here we have assumed that they are not, (2) there is no theoretical reason to suspect that the higher-order moments should be simply proportional to a power of ξ , and (3) though mathematically valid, the expansion of P_0 in terms of ξ_p is not terribly useful in practice.

To illustrate (3) consider the following. One might think that increasingly higher-order moments would be increasingly *irrelevant* for void statistics. In fact, we have explicitly computed the sum in Eqn. 1 for the first eight correlation functions in large galaxy mock catalogs and find that the resulting partial sum in no way approximates the VPF measured from the same mock catalogs. It seems that increasingly higher-order moments are, in fact, increasingly *relevant*.

In order to gain a clearer understanding of this we have investigated the sequence of partial sums of Eqn. 1 using the S_p values given in Eqn. 13. We find that the sequence of partial sums for P_0 oscillates wildly for $p < 20$, but rapidly converges for $p > 25$. In other words, it is not the first few, but the first ~ 25 correlation functions that are necessary to accurately describe the void distribution. Though it is comforting to know that the sum eventually converges, it is quite puzzling why convergence should require so many correlation functions.

One possible explanation for the importance of higher-order moments is the following: since there exist clusters with twenty objects or more, we might expect the 20-point correlation function to be non-zero. This function describes the probability, in excess of random, that a region of space which contains 19 objects will contain a 20th. Since this will almost never happen for a random sample, the 20-point function will likely be quite large, at least on small scales. Hence one might expect contributions from p -point correlation functions as long as there are clusters of objects with p members.

3. METHODOLOGY

We next describe our general methodology for obtaining void statistics from large samples of galaxies. Issues concerning specific survey details, such as the proper handling of angular window functions, are treated as they arise in §§ 5 and 6, where we use data from different surveys.

Investigating the VPF and reduced VPF requires the measurement of three quantities: \bar{N} , $\bar{\xi}$, and P_0 , all of which are functions of the sphere radius, R . Each of these quantities is straightforwardly determined by a counts-in-cells (CIC) approach. One simply places large numbers ($\sim 10^5$) of random spheres within the survey and counts the number of galaxies contained within each sphere. This is then repeated for many sphere radii. \bar{N} is the average number of galaxies in a sphere:

$$\bar{N} = \frac{1}{\mathcal{N}_{tot}} \sum_{i=1}^{\mathcal{N}_{tot}} N_i \quad (14)$$

where \mathcal{N}_{tot} ⁵ is the total number of spheres placed and N_i is the number of galaxies in the i th sphere. P_0 is the number of spheres containing zero galaxies divided by the total number of spheres,

$$P_0 = \frac{\mathcal{N}_0}{\mathcal{N}_{tot}} \quad (15)$$

where \mathcal{N}_0 is the number of spheres that contain zero galaxies, and $\bar{\xi}$ is the variance in the number of galaxies per sphere:

$$\bar{\xi} = \frac{(\overline{N^2} - \bar{N}^2)}{\bar{N}^2} \quad (16)$$

In the limit of large numbers of random points, the CIC approach for determining $\bar{\xi}$ is known to be mathematically equivalent to more conventional methods (Szapudi 1998). We independently confirm this result by comparing our CIC-measured $\bar{\xi}$ to the volume-averaged correlation function obtained via the popular Landy-Szalay

⁵ Here and throughout we use \mathcal{N} to refer to the number of spheres and N to refer to the number of galaxies.

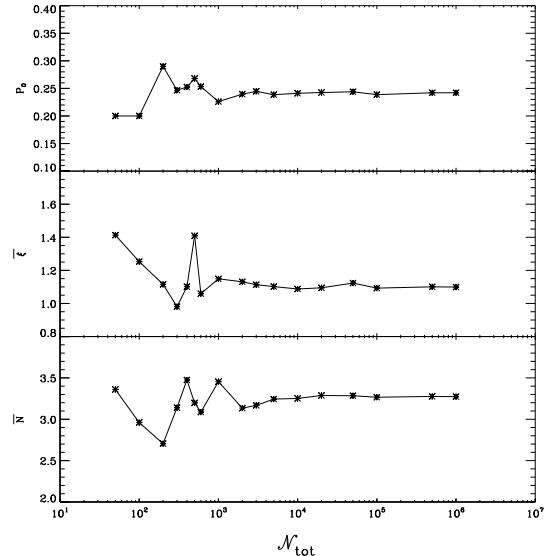


FIG. 2.— Convergence of measured quantities as a function of the number of randomly placed spheres (\mathcal{N}_{tot}) for galaxies in our simulations with a sphere radius of $7 h^{-1}$ Mpc. The rapid convergence is due to the fact that the simulation volume is well-sampled once the number of test volumes exhausts the number of independent configurations, which for this simulation, at a test sphere of $R = 7 h^{-1}$ Mpc, occurs at $\mathcal{N}_{tot} \approx 1500$.

estimator (Landy & Szalay 1993). We find that the two approaches are entirely consistent. To test the sensitivity of these measured quantities to the total number of spheres used, \mathcal{N}_{tot} , we have computed P_0 , \bar{N} , and $\bar{\xi}$ using a sphere radius of $7 h^{-1}$ Mpc, as a function of \mathcal{N}_{tot} (Fig. 2), for mock galaxies in a simulation box of length $256 h^{-1}$ Mpc (see below for simulation details). As expected, for small \mathcal{N}_{tot} , these quantities are unstable, but for $\mathcal{N}_{tot} \gtrsim 10^4$ the quantities converge well. This rapid convergence holds for both smaller and larger void radii and is due to the fact that the simulation volume is well-sampled once the number of test volumes exhausts the number of independent configurations. To be conservative, we use $\mathcal{N}_{tot} \sim 10^5$ to calculate these quantities. Errors for all measured quantities are estimated by “jack-knife” sampling.

Before moving on, we should highlight the fact that all quantities used in analyses of void statistics are spherically averaged. This type of averaging effectively throws away much of the useful information contained in higher order statistics. For example, ξ_3 measures the skewness of the distribution, and will in general *not* be spherically symmetric. Hence it is unclear whether or not spherically averaging ξ_3 is even the proper way to average ξ_3 ; these ambiguities make interpretation difficult.

The $\bar{\xi}$ used here and in other void analyses refers to the correlation function in *redshift space*; the correlation function has not been de-projected into real space, which is the more conventional way of reporting $\bar{\xi}$. This is important because, as we will see, the real space VPF measured in mock catalogs is different from the behavior of the VPF in redshift space, and our main conclusions turn out to be valid only in redshift space. Indeed, Vogeley et al. (1994) find that, at fixed void radii, P_0 in simulations is larger in redshift space compared to real space, with the difference increasing at larger void radii.

These authors also find that redshift space void statistics closely follows one or another hierarchical model (which model the statistics follow depends on gross cosmological models, i.e. closed v.s open and biased vs. unbiased), while the real space void statistics do not. One example of redshift-space effects relevant to this study is the flattening of the S_p scaling coefficients in redshift space when compared to real space. This is due to the reduction of clustering strength on small scales caused by peculiar velocities (known as the fingers-of-God effect). See Bernardeau et al. (2002) for examples of this and other redshift space effects.

Finally, we require that the number density of the sample under consideration be independent of redshift, and so construct volume-limited samples for our analysis. Specifically, we require that each galaxy be observable over the entire redshift range we consider.

4. VOID STATISTICS IN SIMULATIONS

In this section we analyze void statistics in mock galaxy catalogs constructed from N-body Λ CDM simulations in order to help understand and interpret void statistics recovered from observational samples. First we measure the VPF and reduced VPF for dark matter particles and mock galaxies at $z \sim 0$ and $z \sim 1$. We then investigate the reduced VPF for different halo model halo occupation distributions (HODs) and find that they are similar over a wide range of HOD parameters. Next, we determine the effects of redshift space distortions on the VPF and finally we compare VPFs for halo centers alone to VPFs for mock galaxies. Throughout this section we use full simulation boxes at two outputs: $z = 0.087$ (“ $z \sim 0$ ”) and $z = 0.92$ (“ $z \sim 1$ ”); in §5, where we investigate the effects of survey geometry on the VPF, we extract light-cone geometries from the full simulation. Except for §4.3.1, all analyses in this section are performed for galaxies, dark matter particles, and dark matter halos, in redshift space.

4.1. The Simulations

The mock galaxy catalogs we use were constructed specifically for the DEEP2 survey. A complete description of the catalogs is given in Yan, White, & Coil (2004); we give the relevant details here. N-body simulations of 512^3 dark matter particles with a particle mass $m_{part} = 1.0 \times 10^{10} h^{-1} M_\odot$ were run in a Λ CDM universe using the TreePM code (White 2002) in a periodic, cubical box of side length $256 h^{-1}$ Mpc. Dark matter halos were identified by running a “friends-of-friends” group finder. Galaxies were then inserted via a halo model approach, where galaxies are placed in dark matter halos using a simple prescription (see e.g. Seljak 2000; Ma & Fry 2000; Peacock & Smith 2000; Cooray & Sheth 2002; Kravtsov et al. 2004).

The main ingredient of the halo model is the halo occupation distribution, HOD, which specifies the mean number of galaxies to be placed in a given halo, as a function of the halo mass ($\langle N(M) \rangle$). In its most common form the HOD is the sum of a power-law describing the sub-halo (satellite) population and a step function above some minimum mass, which describes the host halo (central galaxy) (Kravtsov et al. 2004). Luminosities are then assigned to galaxies in a halo according to a conditional luminosity function (CLF), $\Phi(L|M)$, which

specifies the luminosity function of galaxies in halos of mass M (Yang et al. 2003). The CLF is traditionally chosen to have a Schechter form. The *same* HOD and CLF are used to populate halos at both high and low redshift, with only the underlying dark matter distribution and the characteristic scale of the luminosity function, L^* , evolving with redshift (evolution in L^* was taken to be 1 mag based on COMBO-17 data (Wolf et al. 2003)). This “no evolution” hypothesis produces catalogs that are in agreement with two-point clustering measurements from DEEP2 at $z \sim 1$ and the B_J -band luminosity function and two-point clustering of 2dF galaxies at $z \sim 0$ (Madgwick et al. 2003). For what we call the ‘primary’ simulations, the specific parameters of the HOD and CLF are chosen to best match the two-point clustering measurements at $z \sim 1$.

4.2. VPF of Dark Matter and Mock Galaxies

This section uses the ‘primary’ simulations as described above. All samples drawn from simulations have been randomly diluted to the same number density ($n = 0.009 h^3 \text{ Mpc}^{-3}$) to allow for a direct comparison between VPF measurements (recall that the VPF, as opposed to the reduced VPF, is quite sensitive to \bar{N}). Furthermore, all galaxies in these samples are restricted to have luminosities $-22 < M_B - 5\log(h) < -19$. Fig. 3 shows the VPF calculated for dark matter particles and galaxies at $z \sim 1$ and $z \sim 0$ in redshift space, where errors are estimated using jackknife sampling. There are two obvious trends. The first is that, at both redshifts, galaxies have a larger P_0 at all radii compared to dark matter, indicating that they are more highly clustered and that galaxies included here are biased relative to the dark matter. This simply results from the fact that these galaxies live in massive dark matter halos that are large overdensities and hence are more highly clustered than the overall dark matter distribution. This is not in conflict with the realization that at $z \sim 0$ the galaxy distribution accurately traces the dark matter on large scales (Verde et al. 2002) because (1) we are probing different scales and (2) these studies have only measured the linear and quadratic bias terms, whereas we are in principle sensitive to all non-linear biasing terms. The second result in Fig. 3 is that both galaxies and dark matter become more clustered with time, as seen by the larger voids at $z \sim 0$ relative to $z \sim 1$; this is due to the effects of gravity.

In Fig. 4 we show the reduced VPF separately for low- and high-redshift mock samples as well as for two hierarchical models, the negative binomial (dashed) and thermodynamic (dash-dot). Here as elsewhere, the upper limit on $\bar{N}\xi$ in the reduced VPF is set by the radius at which $P_0 = 0$; at that point χ becomes undefined. The error on the mean in each point (computed by dividing the cube into octants and measuring void statistics within each octant) is smaller than the plotted symbols (~ 0.001), although errors are highly covariant between different sphere radii. In principle there should be errors on $\bar{N}\xi$ in addition to χ , as $\bar{N}\xi$ will vary across the octants at a specific R . In practice however, the error on $\bar{N}\xi$ is negligible as it is smaller than the binsize.

The dark matter VPF is well described by the thermodynamic model at all scales for both $z \sim 1$ and $z \sim 0$, while the galaxy VPF fits the negative binomial model

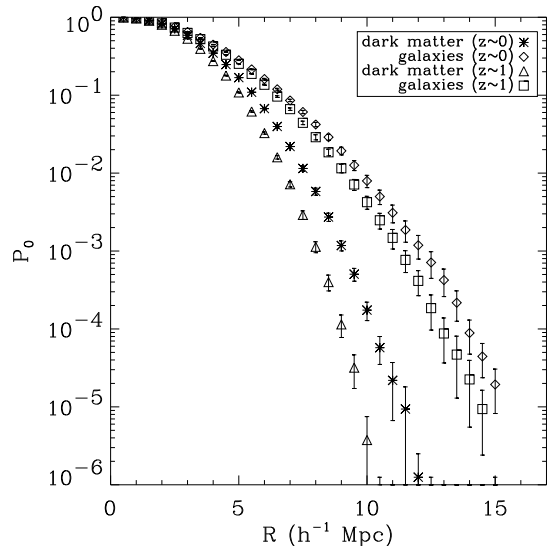


FIG. 3.— VPF (P_0) measured in mock galaxy catalogs and dark matter N-body simulations as a function of comoving radius at $z \sim 1$ and $z \sim 0$. It is apparent that dark matter at $z \sim 0$ (asterisks) has larger voids, and hence is more clustered, than dark matter at $z \sim 1$ (triangles). Similarly, galaxies at $z \sim 0$ (diamonds) are more clustered than galaxies at $z \sim 1$ (squares), and galaxies have more voids than dark matter particles at both epochs. All samples shown here were randomly diluted to a number density of $n = 0.009 h^3 \text{Mpc}^{-3}$, and the mock galaxies were chosen to have luminosities in the range $-22 < M_B - 5\log(h) < -19$.

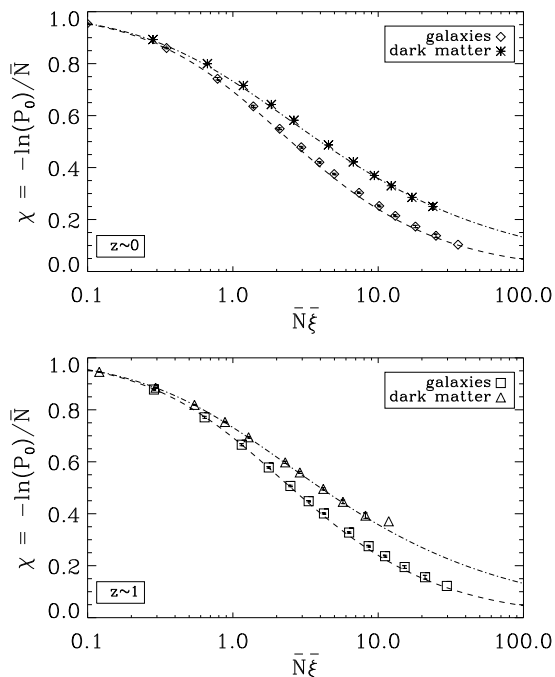


FIG. 4.— Reduced VPF measured in redshift space from simulations at $z \sim 0$ (top) and $z \sim 1$ (bottom). At both redshifts the galaxies follow the negative binomial model (dashed line) while the dark matter follows the thermodynamic model (dot-dashed line). Since all samples have been diluted to the same number density, this implies that the trends seen in Fig. 3 are due solely to changes in the volume-averaged two-point correlation function. See text for details.

to a precision better than the achievable observational errors. In fact, the dark matter matches the thermodynamic model well to at least $z \sim 2$, the highest redshift simulation output available. This directly shows that the VPF can be entirely parameterized in terms of two variables, \bar{N} and $\bar{\xi}$, since, for a given hierarchical model, χ is a function of only of their product (see Eqn. 12). The differences seen in the VPF for galaxies at low and high redshift (Fig. 3) are described entirely by the evolution of $\bar{\xi}$ with cosmic time. Below we find that this dependence holds in the data as well, not only as a function of redshift but also for samples with varying galaxy properties at the same redshifts. Croton et al. (2004) do not find this good agreement between the thermodynamic model and dark matter particles drawn from the Hubble Volume simulations. We speculate that the much larger particle mass ($m_{part} \sim 10^{12} h^{-1} M_\odot$) of these simulations does not afford an accurate measurement of the dark matter particle reduced VPF.

There is a small but perceptible up-turn in the reduced VPF for all samples in Fig. 4 at the largest $\bar{N}\bar{\xi}$ measured. A much larger up-turn has been seen in the CfA survey (Vogeley, Geller, & Huchra 1991; Vogeley et al. 1994) at similar void radii ($7 - 15 h^{-1} \text{Mpc}$, depending on the luminosity threshold). This may be due to fluctuations in the initial conditions of the simulations, as both the galaxies and dark matter at low and high redshift were derived from the same simulation. Furthermore, these large scales (corresponding to void diameters of $\sim 30 h^{-1} \text{Mpc}$) are approaching the limit at which a simulation with box size of $L = 256^3 h^{-3} \text{Mpc}^3$ becomes unreliable due to the fact that large-scale modes, which become increasingly important on larger scales, cannot be included in simulations with periodic boundary conditions. Future studies with different realizations of the initial conditions and larger box sizes will be able to address the significance of this deviation. Regardless, we are unable to probe these largest void scales with the currently available galaxy surveys.

Finally, we find that the good agreement between the reduced VPF in simulations and the negative binomial model is insensitive to random dilutions of the mock galaxies. Specifically, we randomly dilute the mock galaxy catalogs to 25%, 50%, and 75% of the nominal number density and find no differences in the resulting reduced VPFs, as expected since removing dependencies on \bar{N} was a major reason for introducing the reduced VPF in the first place. Defining the VPF as a sum of higher order correlation functions and then inserting the hierarchical *Ansatz* provides a simple explanation for this insensitivity of the reduced VPF on \bar{N} .

4.3. Constraining the Halo Model

As mentioned above, the halo model can be very useful for placing galaxies in cosmological dark matter simulations. It also provides a way of understanding the VPF without resorting to an infinite sum of higher-order correlation functions. Specifically,

$$P_0(V) = \int_0^\infty P(M < M_{min} | \delta_{\bar{m}}) P(\delta_{\bar{m}}) d\delta_{\bar{m}}, \quad (17)$$

where $\delta_{\bar{m}}$ is the mass density contrast smoothed over a volume V , $P(\delta_{\bar{m}})$ is the probability of having a given smoothed mass density contrast, and $P(M < M_{min} | \delta_{\bar{m}})$

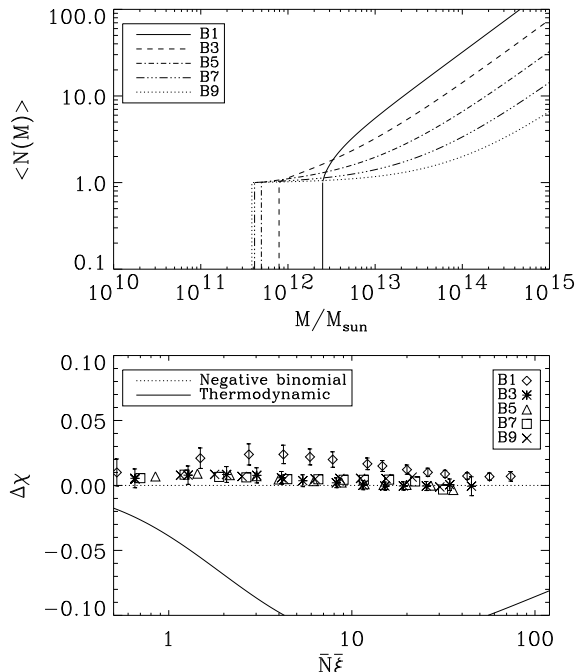


FIG. 5.— *Top*: Various HODs used to populate galaxies in dark matter halos in simulations. *Bottom*: The resulting reduced VPF, in redshift space, for the simulations with the HODs shown in the top panel, plotted as differences from the negative binomial model. The only HOD inconsistent with the negative binomial model, model B1, is easily ruled out observationally by its two-point correlation function. The reduced VPF is almost entirely insensitive to the number of galaxies placed in a halo as a function of galaxy mass. Furthermore, any changes seen in the (un-reduced) VPF can be solely attributed to changes in $\bar{\xi}$. Hence studying the VPF seems to provide no new constraints on the HOD beyond the information available in $\bar{\xi}$.

is the probability of finding a halo with mass less than M_{min} in a volume V with smoothed density contrast $\delta_{\bar{m}}$. Here we have written $P_0(V)$ explicitly as a function of the smoothing volume, but note that it is the same P_0 that occurs elsewhere. The only input from the halo model is the value for M_{min} , the mass above which halos contribute to P_0 . $P(\delta_{\bar{m}})$ is variously assumed in the literature to have a lognormal, negative binomial, or Gaussian distribution, and $P(M < M_{min} | \delta_{\bar{m}})$ is fixed by the relation between halos and dark matter (the halo bias), which can be determined from simulations.

We would like to test the ability of the VPF to constrain the halo model, as suggested by Berlind & Weinberg (2002). Their main results are (1) that the VPF is sensitive to M_{min} , the minimum mass that a dark matter halo must have to host a galaxy, and (2) that the VPF is entirely insensitive to the spatial distribution of galaxies within halos.

To investigate these claims we calculate void statistics, in redshift space, for mock galaxy catalogs constructed from various HODs. The top panel in Fig. 5 shows five different HODs with the simple form (Kravtsov et al. 2004):

$$\langle N(M) \rangle = \begin{cases} 1 + \left[\frac{M - M_{min}}{M_1} \right]^\alpha & \text{for } M > M_{min} \\ 0 & \text{for } M < M_{min} \end{cases}$$

where $\alpha = 0.75$ and $M_{min} = 25.0, 7.9, 4.9, 4.1$ and 3.9 (in

units of $10^{11} h^{-1} M_\odot$). For each M_{min} , M_1 is determined by fixing the overall number density at $0.01 h^3 \text{ Mpc}^{-3}$. These five models are referred to as B1, B3, B5, B7, and B9, respectively.

In order to clearly show small variations between the models, in Fig. 5 (bottom panel) we plot differences between the negative binomial model and the measured reduced VPF for each galaxy catalog. The reduced VPF remains essentially unchanged for these different HODs, leading us to conclude that the VPF can be entirely determined by $\bar{\xi}$, i.e., by Eqn. 12. The scatter between the five models is ~ 0.02 , much smaller than the attainable accuracy with even the largest current galaxy surveys; we therefore conclude that over a wide range of physically meaningful HODs, the VPF cannot constrain M_{min} beyond constraints attainable from $\bar{\xi}$ alone. In the figure, the reduced VPF for the B1 HOD is the most deviant from the negative binomial model. However, observations of the two-point correlation function at $z \sim 1$ (Coil et al. 2005) rule this model out.

These results are consistent with the claims of Berlind & Weinberg (2002), as they were concerned with void statistics in *real space*. The halo model formalism becomes much more complex analytically in redshift space, due to the presence of peculiar velocities. We find using simulations, that redshift-space effects essentially ‘wash out’ any differences in the VPF due to different HODs. Qualitatively, one would expect that placing more galaxies in halos would increase the S_p values on small scales in real space. However, in redshift space, small-scale power is more smeared out because there are now more galaxies residing in massive halos with higher velocity dispersions. It is only a surprise that these two effects should act to cancel each other out exactly. We now investigate the effects of redshift-space distortions on void statistics in detail.

4.3.1. Redshift Space Effects

The effects of redshift space distortions on clustering statistics have been studied in detail (see e.g. Lahav et al. 1993; White 2001; Seljak 2001; Scoccimarro 2004), and have been probed with void statistics (Vogeley et al. 1994; Ryden & Melott 1996). Vogeley et al. (1994) found that voids appear somewhat larger in redshift space and that the reduced VPF in real space does not agree with any of the hierarchical models.

We explore the extent to which redshift-space effects wash away information by calculating the VPF resulting from several HODs with fixed M_{min} and varying α (for $0.5 < \alpha < 1.0$), i.e. varying the number of galaxies placed in halos with mass above M_{min} , while still keeping the overall number density fixed at $0.01 h^3 \text{ Mpc}^{-3}$. One might imagine that, by fixing M_{min} and varying α , P_0 would remain unchanged, but $\bar{\xi}$ would vary because adding more galaxies to a halo will strongly affect the small scale clustering. If this were true, then P_0 would not simply be a function of $\bar{\xi}$ alone. By analyzing a suite of mock galaxy catalogs constructed with these various HODs, we find, as expected, that P_0 remains unchanged. Yet surprisingly, but in accordance with the idea that redshift-space distortions conspire to ‘wash out’ differences due to different HODs, $\bar{\xi}$ remains unchanged for $R \gtrsim 1 h^{-1} \text{ Mpc}$ and is only mildly different for $R \lesssim 1 \text{ Mpc}$. By showing that $\bar{\xi}$ remains the same across differ-

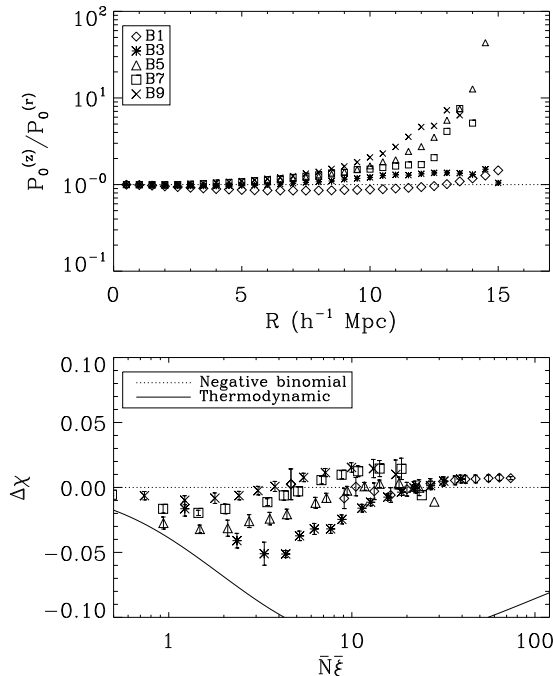


FIG. 6.— Effects of calculating void statistics in real space vs. redshift space. *Top*: Ratio of the VPF, P_0 , in redshift space to real space. There are more voids on large scales in redshift space because of coherent galaxy infall into groups and filaments. *Bottom*: Reduced VPF in real space for mock galaxy catalogs, plotted as differences between the mock galaxies and the negative binomial model. Unlike the reduced VPF in redshift space, here there are trends for different HOD parameters; smaller values of M_{min} agree less well with the negative binomial model than larger values.

ent HODs when P_0 and \bar{N} remain the same, we further solidify our claim that P_0 is solely a function of $\bar{N}\bar{\xi}$, and hence that P_0 does not contain additional information beyond what is available in $\bar{\xi}$.

To quantify the differences between real and redshift space we calculate void statistics for our five HOD models (B1-B9) in real space and compare them to their redshift space analogs. The top panel in Fig. 6 displays the fractional probability increase of the VPF when comparing redshift space ($P_0(z)$) to real space ($P_0(r)$). Two competing effects are at work here: (1) peculiar velocities smear out small scale clustering, and (2) Kaiser infall, due to the coherent infall of structures on larger scales (Kaiser 1987), which has the effect of increasing the size of voids on large scales in redshift space.

The general trends in this figure are consistent with the underlying HOD of each sample. For example, model B1 preferentially places galaxies in higher-mass halos compared to other HODs, and more massive halos have larger velocity dispersions. The larger dispersions decrease the size of voids as seen in redshift space, explaining why there are fewer voids in redshift space compared to real space for the B1 model. This model also has the smallest differences on large scales. This is in part because velocity dispersions are small compared to the largest voids, but also because of Kaiser infall, which increases the apparent size of voids in redshift space on large scales, is important primarily for lower mass halos that are falling into forming structures. Since M_{min} is so large in the B1 model, we expect that most halos in this model are not

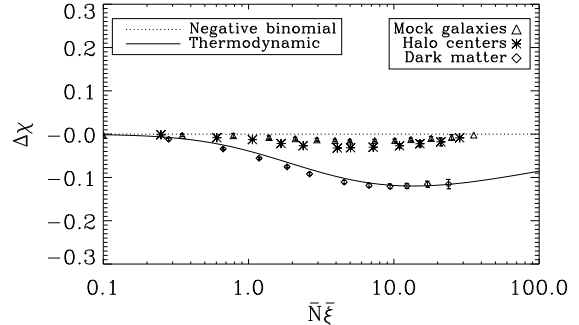


FIG. 7.— Reduced VPF for mock galaxies, dark matter halo centers, and dark matter particles measured in redshift space from the ‘primary’ simulation, plotted as differences from the negative binomial model. It is primarily the clustering properties of dark matter halos, not the galaxies within them, that generates agreement with the negative binomial model.

falling onto forming superstructures.

In the bottom panel of Fig. 6 we see that the reduced VPF can in fact uniquely constrain the halo model when the analysis is performed in real space. The VPF for a set of catalogs can be entirely described by a single function $f(\bar{\xi}, \bar{N})$, and hence cannot be used to uniquely constrain models, if the reduced VPF for those models are all the same. Yet for our five HOD models, this is not the case in real space. Instead, there is a definite trend of χ with M_{min} ; samples with smaller M_{min} are less like the negative binomial model. On larger scales ($\sim 5 h^{-1}$ Mpc) the HODs are again indistinguishable, as is expected since HOD parameters are relevant only on halo scales (i.e. $\sim 1 h^{-1}$ Mpc). Although it seems intuitive that the VPF should be capable of uniquely constraining the HOD (specifically M_{min}), redshift-space effects make this extremely difficult in practice.

4.3.2. VPF for Dark Matter Halos

We can better understand the insensitivity of the VPF to particular parameters of the HOD by considering the VPF for the *centers* of dark matter halos (restricted to have $M_{halo} > M_{min}$) alone. Fig. 7 compares the reduced VPF for dark matter particles, dark matter halo centers, and mock galaxies. As the figure indicates, it is primarily the clustering properties of dark matter halos, not the number of galaxies within them, that generates agreement with the negative binomial model.

We find the similarity in reduced VPF for halo centers and mock galaxies intuitive for two reasons. First, as most dark matter halos in our simulations with $M > M_{min}$ contain a single isolated galaxy, and galaxies in most halo models are placed first in the center of the halo, it is reasonable that the clustering of halo centers has more impact on the galaxy reduced VPF than α . Second, when more than one galaxy is placed in a halo, it is typically within $\sim 500 h^{-1}$ kpc of the halo center, as very few halos have larger radii. Hence a sphere containing a satellite galaxy will typically already include the galaxy at the halo’s center. This also explains why void statistics are insensitive to the spatial distribution of galaxies within halos, as noted by Berlind & Weinberg (2002).

In conclusion, the VPF does not seem to be capable of providing competitive constraints on the major parameters of the HOD. This is due both to redshift space distortions washing out information on small scales and to the fact that the clustering of dark matter halos alone dominates the VPF. Although one might have thought that the VPF for galaxies and halos would be uniquely sensitive to M_{min} , it turns out that any changes in M_{min} are likewise reflected in ξ , in a way that can exactly account for changes in the VPF.

5. VOID STATISTICS FROM DEEP2

We now measure void statistics in state-of-the-art redshift surveys that are mapping the three-dimensional positions of thousands of galaxies. In this section we probe void statistics when the universe was roughly half its present age ($z \sim 1$). In the following section we focus on voids in the local universe ($z \sim 0$).

5.1. The Data

The DEEP2 Galaxy Redshift Survey (Davis et al. 2004) is an ongoing project that is gathering optical spectra for $\sim 50,000$ galaxies at $z \sim 1$ using the DEIMOS spectrograph on the Keck II 10-m telescope. The completed survey will span a comoving volume of $\sim 10^6 h^{-3} \text{ Mpc}^3$, covering 3 deg^2 over four widely separated fields; observations began July 2002 and are expected to be completed in mid-2006. Due to the high dispersion and excellent sky subtraction provided by the DEIMOS spectrograph ($R \sim 5,000$), our rms redshift errors, determined from repeated observations, are $\sim 30 \text{ km s}^{-1}$, minuscule compared to void scales.

Target galaxies are selected using *BRI* imaging from the CFHT telescope down to a limiting magnitude of $R = 24.1$ (all magnitudes in this paper are in the AB system; see Coil et al. 2004 for photometric details). In three of the four fields we also use apparent colors to exclude objects likely to have $z < 0.7$. This pre-selection greatly enhances our efficiency for targeting galaxies at high redshift (Newman et al. 2005). A fourth field, the Extended Groth Strip (EGS), has no redshift pre-selection, and is not used in the present analysis. For galaxies with a successfully identified redshift, absolute *B*-band magnitudes (M_B) and restframe $U - B$ colors, denoted $(U - B)_0$, have been derived (Willmer et al. 2005). In the discussion below, we define “red” and “blue” galaxies according to whether $(U - B)_0 > 1$ or $(U - B)_0 < 1$; this roughly corresponds to the saddle point of the color bimodality observed in DEEP2 data (Willmer et al. 2005). The current study uses 12,000 redshifts with $0.75 \gtrsim z \lesssim 1.0$ in three fields covering $\sim 2.2 \text{ deg}^2$. The three fields we use correspond to the DEEP2 pointings 21, part of 22, 31, 32, 33, 41, and 42, as defined in Coil et al. (2004a).

An important aspect in analysis of any large-scale galaxy survey is the proper handling of selection effects that may vary as a function of galaxy property, such as color and luminosity. DEEP2 is an *R*-band limited survey, which corresponds to restframe UV at $z > 1$, and results in fewer red galaxies being targeted at higher redshift compared to blue galaxies (Willmer et al. 2005). Due to this selection effect and the generally lower sampling density beyond $z \sim 1$, we limit our analysis in this study to $z < 1$.

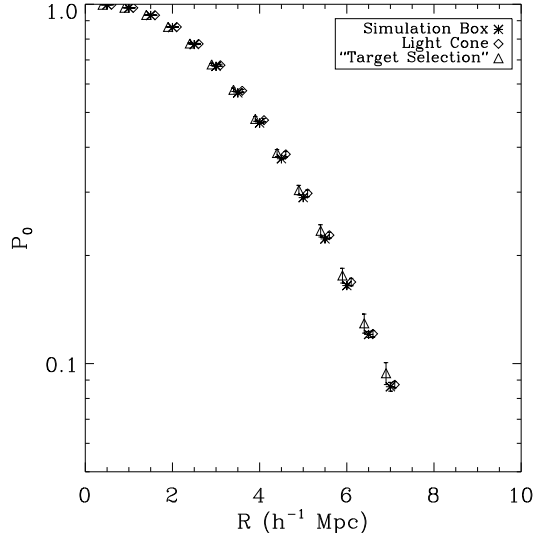


FIG. 8.— VPF, P_0 , for mock galaxies with $-22 < M_B - 5\log(h) < -19$ and a number density of $0.006 h^3 \text{ Mpc}^{-3}$. P_0 values are for galaxies in the full simulation box at $z \sim 1$ (stars), galaxies in a lightcone with the same geometry as the DEEP2 survey sample in this paper (diamond), and galaxies in the light cone that have passed the DEEP2 target selection criteria (triangles). See the text for details. The points have been offset from each other to make the plot more readable; each set of points is based on spheres of the same radius. Error bars are obtained from averaging over three mock light cones, which correspond to the three separate DEEP2 fields.

5.1.1. Survey Geometry and Completeness

Each DEEP2 field is much longer in the redshift direction than on the sky; the $1 - 2 \times 0.5 \text{ deg}^2$ fields used for this work span $40 - 80 \times \sim 20 h^{-1} \text{ Mpc}$ in transverse comoving extent, while the range $0.7 < z < 1.0$ corresponds to $560 h^{-1} \text{ Mpc}$ comoving in the redshift direction. The number of possible independent spheres contained within the survey, as indicated by V_{survey}/V_{sphere} , varies from $\sim 10^5$ for $1 h^{-1} \text{ Mpc}$ spheres to $\sim 10^3$ for $7 h^{-1} \text{ Mpc}$ spheres.

One might be concerned that the survey geometry would skew void statistics when probing voids with diameters comparable to the short dimension of the survey. We have tested this effect by comparing the VPFs from a full mock galaxy simulation box at $z \sim 1$, constructed from the ‘primary’ simulation (see §4.1), to mock galaxy catalogs with a “lightcone” geometry similar to DEEP2. The lightcone geometry is constructed by stacking together several simulation box outputs and slicing through them diagonally, so as not to pick up the same structures at different times.

We find that, even at the largest radii tested, the VPF in the mock lightcone and larger simulation box agree to within 1σ (Fig. 8). Of course, due to the decrease in the number of independent volume elements at large void radii, cosmic variance increases, and hence the scatter (computed across three mock light cones) increases. We conclude that the geometry of the DEEP2 survey allows us to accurately probe voids to radii of at least $7 h^{-1} \text{ Mpc}$ comoving.

Another selection effect is the survey completeness. The DEEP2 survey spectroscopically targets $\sim 60\%$ of

objects that pass the apparent magnitude and color cuts mentioned above. Of those targeted objects, we are able to secure redshifts for $> 70\%$. Follow-up observations have shown that $\sim 10\%$ of the targets are objects at $z > 1.5$ (C. Steidel, private communication). We therefore have successful redshifts for $\sim 50\%$ of all galaxies at $0.75 < z < 1.0$ in the surveyed fields with apparent magnitude of $R < 24.1$. This sampling rate is effectively scaled out when we dilute the mock galaxy catalogs to compare to the DEEP2 data. Further complications arise because the sampling rate is non-uniform due to the necessities of slitmask design. Spectra of objects are not allowed to overlap on the CCD, such that objects that lie near each other in the direction on the sky that maps to the wavelength direction on the CCD can not be simultaneously observed; this results in modest ($\lesssim 10\%$) under-sampling in regions with the highest density of targets on the plane of the sky (each point on the sky is covered by multiple DEEP2 slitmasks to ameliorate this effect). We model this effect by applying the actual DEEP2 maskmaking algorithm to the mock galaxy catalogs and then computing the VPF. We find that the impact of the target selection algorithm on the VPF is negligible to within 1σ (see Fig. 8). One would have expected this, as the effect is most relevant on small scales and in overdense regions.

There are also selection effects due to bright stars and other regions that were not observed. These result in inhomogeneities on much larger scales ($\gtrsim 1$ Mpc) that could potentially be more relevant for void studies. To take account of these effects for the DEEP2 sample, we generate an angular window function that has, for each right ascension and declination, the completeness at that point determined from the bad-pixel masks used in making our photometric catalogs and the observed redshift success for slitmasks covering that point. This window function therefore masks unobservable regions such as areas around bright stars (they are given a completeness of 0.0). We then convolve this window function with a circular kernel proportional to the path length through a sphere of radius R projected on the sky (i.e., $K(\Delta\alpha, \Delta\delta) \propto \sqrt{\rho^2 - (\Delta\alpha)^2 - (\Delta\delta)^2}$, where ρ is the projected radius of the sphere in arcseconds, and $\Delta\alpha$ and $\Delta\delta$ are the separations on the sky from the center of the kernel in the right-ascension and declination directions, respectively).

This convolution has a simple physical consequence: we treat a test sphere completely inside the survey volume at a region of 50% completeness as equivalent to a sphere only 50% in the survey volume at a region of 100% completeness. Our final product is a window function that contains, at each point, the projected completeness averaged over a sphere of a given radius, weighting by the path length through the sphere. We then throw down random spheres only at points above a minimum convolved completeness. This allows us to robustly avoid regions of bright stars, regions of low completeness (due, for example, to bad weather during observations) and the edges of the survey. For DEEP2, we set the completeness threshold at 55% so that the allowable completeness range varies over the survey by $\lesssim 10\%$. It is more important for our purposes to be *uniformly* complete than highly complete, as an overall dilution of the sample does

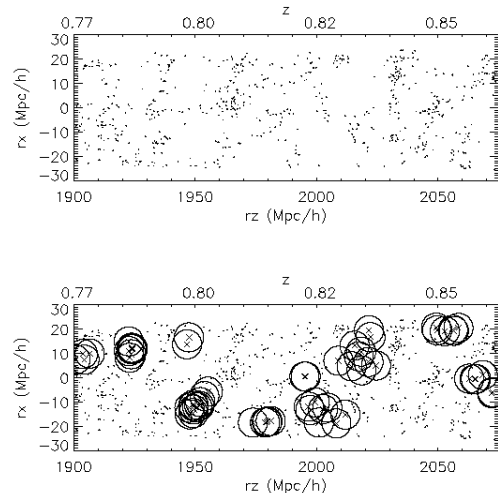


FIG. 9.— Schematic demonstration of the statistical nature of the VPF. The top panel shows the comoving projected positions for galaxies in a section of one DEEP2 field. The suppressed dimension is $\sim 10 h^{-1}$ Mpc thick. The bottom panel shows the empty spheres found with a search radius of $6 h^{-1}$ Mpc. We show a very small fraction of the actual number of empty spheres detected at this radius for clarity.

not effect the reduced VPF.

We test the accuracy of this method by dividing the measured average number of galaxies in a sphere of radius R , \bar{N} , by the sphere volume for each radius. We find that this inferred number density is constant with sphere radius, providing good evidence that the larger spheres do not tend to lay farther outside the survey geometry than smaller spheres. Finally, we have spot-checked by eye the locations of the largest voids to ensure that they fall within the survey geometry (see Fig. 9).

5.2. Results at $z \sim 1$

We investigate the VPF and reduced VPF for DEEP2 galaxies in three ways. First we consider an “overall” sample consisting of all galaxies with $-22 < M_B - 5\log(h) < -19$ and $0.75 < z < 1.0$. Then we compute the VPF as a function of galaxy color and of luminosity, using volume-limited samples. Errors for all DEEP2 measurements were derived from jackknife sampling using subvolumes of the three widely separated DEEP2 fields.

We find excellent agreement between the overall DEEP2 sample VPF and the mock galaxy catalog VPF (Fig. 10, top panel). The mock catalogs were randomly diluted to have the same number density ($n = 0.006 h^3 \text{Mpc}^{-3}$) as the DEEP2 overall sample. The dashed line is a prediction of the negative binomial model. We show the reduced VPF, plotted as differences from the negative binomial prediction, for the overall sample in the top panel of Fig. 11, top panel. The good agreement between the data and the model implies that the VPF can be described entirely by \bar{N} and ξ . The largest deviations on large scales seen here and below are of low statistical significance; the data are highly covariant from bin to bin, and hence our errors are underestimates of the true error. The excellent agreement between the overall sample and mock galaxy VPF reflects the fact that the mock galaxy catalogs were constructed to match the ob-

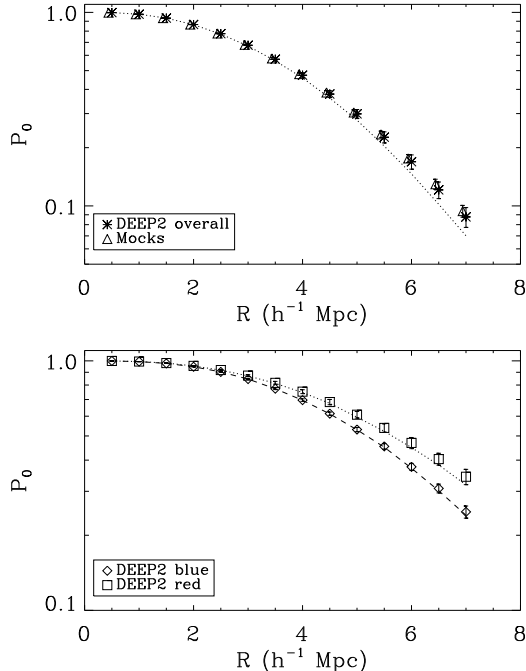


FIG. 10.— *Top*: P_0 for the overall DEEP2 sample compared to mock galaxy catalogs. The mock catalogs have an identical geometry as the DEEP2 survey volume and have been passed through the DEEP2 target selection algorithm. Both samples have the same number density ($n = 0.006 h^3 \text{ Mpc}^{-3}$). The good agreement between the mock catalogs and the data, although on the surface encouraging, is due entirely to the fact that the mock catalogs were constructed to match the DEEP2 two-point correlation function (see text for details). *Bottom*: DEEP2 P_0 separately for red and blue galaxies, both diluted to $n = 0.002 h^3 \text{ Mpc}^{-3}$. The dilution removes any number density effect on the VPF, implying that we are only seeing effects of clustering on the VPFs shown here. Lines are predictions of the negative binomial model.

served $\bar{\xi}$ in the DEEP2 data. Stated differently, since these samples have the same number density (by construction), the fact that they have similar VPFs implies that they will have similar $\bar{\xi}$ values, and vice versa.

We next divide the DEEP2 sample into galaxies with $(U - B)_0 < 1$ or > 1 , roughly matching the observed saddle point in the color bi-modality. We find that samples of red galaxies have more and/or larger voids than samples of blue galaxies (Fig. 10, bottom panel; both samples were randomly diluted to $n = 0.002 h^3 \text{ Mpc}^{-3}$). This dilution is critical; without it, the differences between the red and blue galaxy VPF would be dominated by differences in the observed number density of red versus blue galaxies. It would be very difficult to separate the effects of number density from clustering strength on the number and size of voids if we simply compared the VPFs of undiluted samples.

As with the overall sample, we find that the reduced VPF of both the blue and red galaxy populations follows the negative binomial model within the errors (Fig. 11, top panel). Again, this implies that the differences between the VPFs for blue and red galaxies (Fig. 10, bottom panel) are solely due to differences in their two-point correlation functions. The similarity in reduced VPFs is somewhat surprising. We know that blue and red galaxies are biased differently relative to the dark matter (e.g.,

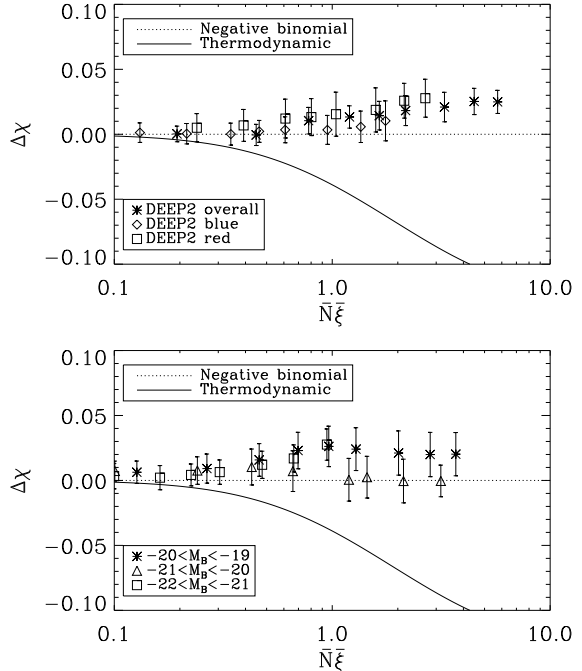


FIG. 11.— Reduced VPF for DEEP2 galaxies, plotted as differences between the negative binomial model and the data. *Top*: Differences for the overall, red, and blue samples. The data are consistent with the model. *Bottom*: Differences for the DEEP2 sample in differential magnitude bins. Again there is good agreement between the data and the model. The deviations on the largest scales are likely insignificant due to the large covariance between bins, which results in an underestimate of the true error.

Zehavi et al. 2002; Coil et al. 2004b, 2005, and references therein), and that the S_p values are dependent on the bias. We might have expected the reduced VPFs, which according to Eqn. 6 should depend on the S_p values, to be different for these two populations.

The halo model affords a more direct interpretation of these results. We have seen in § 4.3 that the reduced VPF is insensitive to parameters of the HOD. From studies of galaxy correlations at $z \sim 0$, it is becoming apparent that different populations of galaxies can have very different HODs. Hence the result that red and blue galaxies have similar reduced VPFs is consistent with our tests using mock catalogs; very different HODs will still produce the same reduced VPF.

We also investigate the DEEP2 VPF dividing the sample into three luminosity bins: $-20 < M_B < -19$, $-21 < M_B < -20$, and $-22 < M_B < -21$. We take a slightly different approach for this analysis. Since the number densities of the three luminosity subsamples vary by roughly a factor of four, the dilution required for a direct comparison of VPFs can discard a great deal of information and unnecessarily increases Poisson errors. For this reason, we begin by analyzing the reduced VPF for each luminosity sample (Fig. 11, bottom panel), again finding good agreement with the negative binomial model. Using this model, we can then use Eqn. 12 to predict the VPF at any radius based solely on our knowledge of \bar{N} and $\bar{\xi}$ at that radius. In Fig. 12 we plot the VPF for each of the three magnitude bins (without diluting the number density) and also show the predictions based

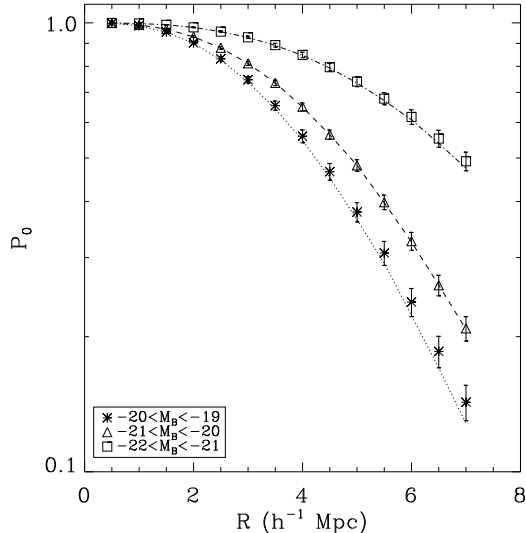


FIG. 12.— Plot of P_0 for DEEP2 galaxies as a function of luminosity. The competing effects due to the number density and clustering strengths drive the differences between subsamples. Given that the reduced VPF for these subsamples can be characterized by the negative binomial model (see Fig. 11), we predict P_0 for each sample using only the number density and volume-averaged two-point correlation function measured within spheres of the given radius (lines). The excellent agreement seen here between the data and the predictions simply reflects the agreement found in Fig. 11 (bottom).

on the negative binomial model; again, the agreement is within the errors. Knowledge of the form of the reduced VPF allows us to separate the effects of number density from clustering on the VPF.

We note that the three magnitude bins cover slightly different redshift intervals. While the faintest bin ($-20 < M_B - 5\log(h) < -19$) spans $0.7 < z < 0.85$, the brightest bin ($-22 < M_B - 5\log(h) < -21$) spans $0.83 < z < 1.05$. Each redshift interval is chosen such that the sample being considered should have a roughly constant number density as a function of redshift. This ensures that there is no artificial redshift dependence in the void distribution; i.e., the samples are volume limited. The less luminous galaxies have a constant number density only over a limited redshift range because they have $R > 24.1$ at higher redshifts.

The reduced VPF of all populations of galaxies at $z \sim 1$ is well fit by the negative binomial model. Hence the VPF, a statistic that in principle relies on the infinite hierarchy of correlation functions, can in fact be accurately described solely by the number density and the volume-averaged two-point correlation function of the sample. We conclude that, at $z \sim 1$, the VPF provides no constraints on either the halo model or on cosmological parameters that cannot be gleaned from studies of correlation statistics.

6. VOID STATISTICS FROM SDSS

6.1. The Data

The Sloan Digital Sky Survey (SDSS; York et al. 2000; Abazajian et al. 2004) is an extensive photometric and spectroscopic survey of the local universe. Imaging data exist over 10^4 deg^2 in five bandpasses, $u, g, r, i,$ and z . We use color conversions provided by M. Blanton (private

communication) to derive B -band magnitudes in the AB system, with typical $1\text{-}\sigma$ errors in the conversion of 0.2 magnitudes. Approximately 10^6 objects are being targeted for follow-up spectroscopy as part of the SDSS; most spectroscopic targets are brighter than $r = 17.77$ (Strauss et al. 2002). Automated software performs all the necessary data reduction, including the assignment of redshifts. Redshift errors are $\sim 30 \text{ kms}^{-1}$, similar to DEEP2. The spectrograph tiling algorithm ensures nearly complete sampling (Blanton et al. 2003a), yet the survey is not 100% complete due to several effects: (1) fiber collisions that do not allow objects separated by $< 1'$ to be simultaneously targeted, affecting $\sim 6\%$ of targetable objects, (2) a small fraction ($< 1\%$) of targeted galaxies fail to yield a reliable redshift, and (3) bright Galactic stars block small regions of the sky. Unlike the DEEP2 survey, (3) is not as important for SDSS because a bright star will block out a much smaller comoving volume at $z \sim 0$ compared to $z \sim 1$. The first of these effects is only important on small scales, and is likely negligible for void statistics since an undersampled, intrinsically high density region will not be counted as a void.

For this analysis we make use of the hybrid NYU Value Added Galaxy Catalog (VAGC) (Blanton et al. 2005). This catalog combines the SDSS Data Release 2 with a multitude of other publicly available catalogs (2dF, 2MASS, IRAS PSCz, FIRST, and RC3), and includes a variety of derived parameters including K -corrections (Blanton et al. 2003b) and structural parameters.

From the VAGC we have selected the two largest contiguous regions of the SDSS. We will call *SDSS1* the region at $\alpha = 190^\circ$, $\delta = 50^\circ$, which includes $\sim 103,000$ galaxies with spectroscopic $z < 0.2$ and *SDSS2* the region centered on $\alpha = 190^\circ$, $\delta = 1^\circ$ with $\sim 87,000$ galaxies at $z < 0.2$. We divide red and blue galaxies in the SDSS data at the valley visible in the rest-frame $g - r$ color distribution at $(g - r) = 0.7$.

In addition to the ‘main’ SDSS sample there is a secondary targeting algorithm designed to identify large numbers of luminous red galaxies (LRGs) at moderate redshifts via photometric color cuts. These LRGs, though low in spatial number density, cover an enormous volume, and are hence ideal objects for measuring very large scale clustering in the universe (see Zehavi et al. 2005b; Eisenstein et al. 2005, for a more detailed description of the SDSS LRG sample). The LRG sample we study here contains $\sim 10,000$ galaxies and spans the redshift range $0.16 < z < 0.46$ and luminosity range $-23.2 < M_g < -21.8$ with $(g - r) > 0.7$ (note that this is the only case where we use SDSS absolute magnitudes).

6.1.1. Survey Geometry and Completeness

Since the SDSS is a low-redshift survey, the angular size of a test void sphere of the same comoving radius varies enormously over the redshift range $0.05 < z < 0.2$. Paralleling our analysis of the DEEP2 sample, we account for geometry and completeness effects in the following way. We generate an angular window function for the SDSS with the aid of *Mangle* (Hamilton & Tegmark 2004) over a dense grid in right ascension and declination; the resulting resolution is 0.15 degrees in right ascension and declination. Completeness values of either 0 or 1 were assigned to each right point of this grid de-

pending on the spectroscopic coverage and locations of bright stars (as SDSS spectroscopy is highly uniform in depth). We then convolve this window function with a kernel that represents the depth through the test void projected on the sky (see § 5.1.1 for details) and only place random spheres in regions above a minimum convolved completeness. This allows us to avoid placing test spheres in poorly-sampled regions. We set this threshold at 85%, so that the completeness within spheres placed down varies over the survey by $\lesssim 10\%$.

The net result of the strong scaling of angular size with redshift is that larger-volume test spheres cannot be placed in the lowest redshift bins because they would span a region of the sky comparable to the entire survey. Hence at larger void radii we are restricted to higher redshifts. This does not cause a detrimental bias, however, because we only consider galaxies over a redshift range such that their number density is approximately constant, i.e., volume-limited samples. Hence a bias towards slightly higher redshifts ($z \sim 0.1$) for larger voids will not skew our statistics, assuming that there is not strong void statistic evolution from $z \sim 0$ to $z \sim 0.1$. Indeed no significant evolution has been detected in the VPF out to $z \sim 0.3$ (Hoyle & Vogeley 2004).

There is one final effect in the SDSS data that, if not properly treated, could significantly bias our results. There is a massive structure in *SDSS2* at $z \sim 0.08$ dubbed the ‘‘Sloan Great Wall’’ (Gott et al. 2005), which will strongly affect any clustering measurements. This structure has been removed in the correlation function studies of Zehavi et al. (2002), and we do the same here by defining our samples to avoid $0.075 < z < 0.085$ in the *SDSS2* sample. The structure extends across the entire angular extent of *SDSS2*; if included it would cause gross underestimates of the cosmic error in any large-scale structure measurement. Based on many realizations of large cosmological simulations with Gaussian initial conditions, it is expected that a structure of this size occurs in a volume the size of the SDSS approximately 10% of the time (Tegmark et al. 2004). With the full SDSS dataset, it should be possible to accurately account for this enormous structure in the error budget without relying on simulations.

In order to accurately measure quantities via our counts-in-cells approach, it is important that the number of randomly placed test spheres exhausts the number of independent volumes in the survey. The second data release of the SDSS over the interval $0.8 < z < 0.15$ spans a volume of $\sim 10^7 h^{-3} \text{Mpc}^3$. This corresponds to $\sim 10^6$ independent volumes for $1 h^{-1} \text{Mpc}$ spheres and $\sim 10^3$ for $15 h^{-1} \text{Mpc}$ spheres, a factor of 10 more than in the DEEP2 survey. The number of spheres we use always exceeds the number of independent volumes.

6.2. Results at $z \sim 0$

We now present void statistics in the local universe using the SDSS dataset. As in our analysis of DEEP2 data, we investigate void statistics for three sets of SDSS samples: an ‘‘overall’’ sample with $-22 < M_B - 5\log(h) < -19$ and $0.09 < z < 0.14$, two subsamples split according to $g - r$ color (at $(g - r) = 0.7$), and three subsamples differing in luminosity. In this section, as before, we plot reduced VPFs as differences from the negative binomial model in order to clearly show small deviations.

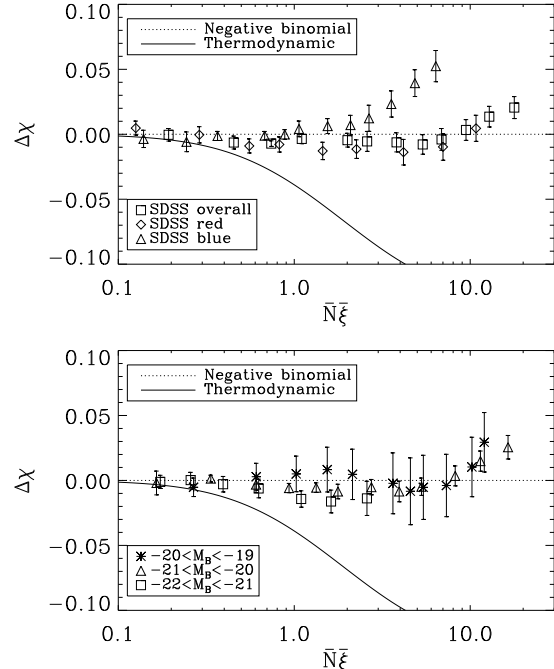


FIG. 13.— Reduced VPF for SDSS galaxies, plotted as differences from the negative binomial model. *Top*: The overall, blue, and red galaxy samples agree well with the negative binomial model. The largest discrepancy is for blue galaxies, although due to the large covariance between bins, these errors are underestimates of the true error. *Bottom*: Reduced VPF for SDSS galaxies as a function of luminosity. All luminosity classes agree well with the model, with the largest deviations seen in the intermediate luminosity sample.

As for the DEEP2 luminosity subsamples, All comparisons made in this section are made without requiring that samples have similar number densities, and by using the negative binomial model to predict the VPF (via Eqn. 12). Errors for all quantities were derived from jackknife subsamples.

The reduced VPFs for the overall, red, and blue samples (Fig. 13, top panel) are all well described by the negative binomial model. As in the previous sections, we can use this measured agreement to predict the VPF at any radius based solely on \bar{N} and ξ for that radius, (e.g. as estimated from counts-in-cells), for each sample. Fig. 14 (top panel) plots the VPF for these samples and compares them to the predictions from the negative binomial model (lines). The trend that the red galaxy sample has more and/or larger voids than the blue sample is due to the fact that it is both more strongly clustered and lower in number density than our sample of blue galaxies. That the measured data agree with the negative binomial model within errors implies that, just as at $z \sim 1$, the VPF cannot be used to uniquely constrain the halo model or cosmological parameters. As with the overall DEEP2 VPF, the blue SDSS data do not agree within 1σ errors on the largest scales; this is likely insignificant, as the data are highly covariant, and hence our errors are underestimates of the true error.

Next, we compare void statistics for samples of SDSS galaxies as a function of luminosity. The reduced VPF for galaxies in all luminosity bins we consider ($-22 < M_B - 5\log(h) < -21$, $-21 < M_B - 5\log(h) < -20$, and

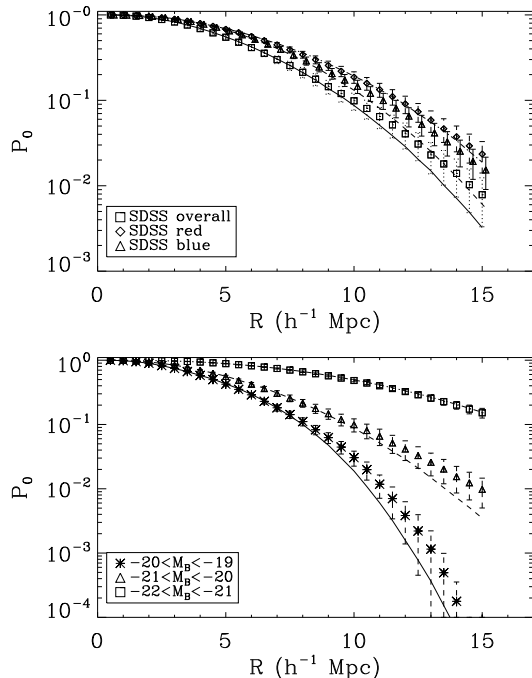


FIG. 14.— Plot of P_0 measured for SDSS galaxies, overall and as a function of color (*top*) and luminosity (*bottom*). The data are shown as points, while lines are predictions from the negative binomial model for each subsample. The predictions are determined from measurements of \bar{N} and $\bar{\xi}$ for spheres as a function of radius. The agreement implies that \bar{N} and $\bar{\xi}$ alone determine P_0 .

$-20 < M_B - 5\log(h) < -19$), is in good agreement with the negative binomial model (Fig. 13, bottom panel). We again make this agreement explicit by computing the VPFs for these samples and comparing to that predicted by assuming the negative binomial model from the values of \bar{N} and $\bar{\xi}$ (Fig. 14, bottom panel). Since these samples are volume limited, each luminosity sample spans a slightly different redshift range, with the brightest spanning the largest range ($0.11 < z < 0.20$) (since bright galaxies can be detected at greatest distances) and the faintest spanning the smallest range ($0.05 < z < 0.07$).

Finally, we compute the VPF for the LRG population, defined to be bright ($-23.2 < M_g < -21.8$) and red ($(g-r) > 0.7$), spanning the redshift range $0.16 < z < 0.46$. Their low number density ($n \sim 10^{-5} h^3 \text{ Mpc}^{-3}$) and large redshift range allow for a measurement of the VPF out to unprecedented scales ($R=40 h^{-1} \text{ Mpc}$). Fig. 15 shows that the LRG population is well described by the negative binomial model out to the largest void radii tested. Unlike our analysis of other SDSS data, we plot the VPF separately for the two regions used in this study (denoted *SDSS1* and *SDSS2*). The difference between the two regions reflects the impact of cosmic variance on void statistics.

The reduced VPFs of all galaxy populations explored at $z \sim 0$ are in good agreement with the negative binomial model. It is quite surprising that this agreement, which provides a simple mapping from \bar{N} and $\bar{\xi}$ to P_0 , is equally valid from $z \sim 1$ to $z \sim 0$. What this tells us is that the evolution in the VPF for a given population from $z \sim 1$ to $z \sim 0$ must proceed in lockstep with evolution in the number density and two-point cor-

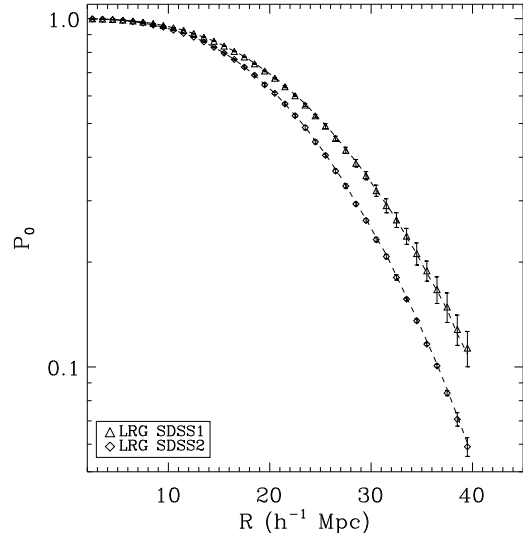


FIG. 15.— Measured P_0 for the SDSS LRG population over the redshift range $0.16 < z < 0.46$. Unlike for the other SDSS data samples, here we are able to measure P_0 to much larger radii and therefore show results separately for each of the two SDSS regions on the sky, denoted *SDSS1* and *SDSS2* (see §6.1). The difference between the two regions reflects the cosmic variance of their volumes. As before, we show jackknife error estimates. The negative binomial predictions (lines) match the measured P_0 values well out to void radii of $40 h^{-1} \text{ Mpc}$.

relation function of that population. Finally, it is encouraging that these conclusions at $z \sim 0$ agree with Croton et al. (2004), who measure void statistics for the low-redshift 2dF survey, and find good agreement between the galaxy reduced VPF and the negative binomial model for a range of galaxy luminosities.

7. DISCUSSION

We have presented measurements of the void probability function (VPF) and reduced VPF for galaxies as a function of color and luminosity at $z \sim 1$ using DEEP2 data and at $z \sim 0$ with SDSS data. We find that all samples are well described by the negative binomial model. This agreement implies that the VPF for a given sample is determined entirely by the sample number density and volume-averaged two-point correlation function, $\bar{\xi}$. In particular, evolution of the VPF for a population of galaxies from $z \sim 1$ to $z \sim 0$ is governed by the evolution in $\bar{\xi}$ and \bar{N} for that population. We have furthermore shown, using mock catalogs, that this simple relation between the VPF and $\bar{\xi}$ holds for a wide range of halo models in redshift space, but breaks down in real space. We now discuss the relevance and implications of these findings.

The VPF we measure at $z \sim 1$ is in good agreement with the VPF measured in mock galaxy catalogs created from Λ CDM simulations. Although this is encouraging, our result that the two-point correlation function and number density determine the VPF implies that this agreement found between data and simulations is simply a consequence of the fact that the simulations were constructed to match the number density and two-point correlation function of DEEP2 galaxies. Stated differently, the VPF currently cannot provide new constraints either on cosmological parameters or on the method in which

galaxies are placed into dark matter N-body simulations.

Previous void studies have interpreted the VPF according to its mathematical expansion as an infinite sum of higher-order correlation functions, using the hierarchical *Ansatz* to relate the higher-order functions to lower-order functions. These studies then attempt to use the reduced VPF to test the validity of this *Ansatz*. Strictly speaking, however, finding that the VPF for various populations of galaxies can be characterized entirely by \bar{N} and $\bar{\xi}$ does *not* provide evidence for the validity of this *Ansatz*. In fact, the interpretation of the VPF in terms of higher-order correlation functions implies that the reduced VPF depends only on the scaling coefficients ($S_p \equiv \xi_p/\xi^{p-1}$), which suggests that populations with different biases (and therefore different scalings between the three-point and two-point functions) should actually not have the same reduced VPF. We find just the opposite in the data, namely that populations with different biases have the same reduced VPF. The interpretation of the VPF as a sum of correlation functions affords little insight into these results. Despite this, the interpretation predicts that the reduced VPF of a sample should be independent of that sample's number density, and this is indeed observed.

The halo model provides a more tractable theoretical framework. We have shown that the reduced VPF of mock galaxies is quite insensitive to particular parameters of the HOD when voids are measured in redshift space. Using measurements of ξ to constrain the halo model, it appears that blue and red galaxies have very different HODs (Zehavi et al. 2005a). The samples we investigate here hence likely have a range of HODs. Yet, based on the result that different HODs generate the same reduced VPF, it is not surprising that different samples have the same reduced VPF.

Furthermore, an analysis of the dark matter *halo* reduced VPF has led us to conclude that it is the redshift-space distribution of halos themselves that is primarily responsible for the agreement between the measured reduced VPF and the negative binomial model. The reduced VPF changes very little when one populates dark matter halos with galaxies. It is only surprising that the minimum halo mass, M_{min} , has very little effect on the reduced VPF as well. This insensitivity to M_{min} implies that the changes in $\bar{\xi}$ caused by changes in M_{min} are enough to completely account for the changes in the VPF.

We would like to stress that the strict dependence of the VPF on $\bar{N}\bar{\xi}$ does not rely on any theoretical interpretation, including the hierarchical *Ansatz*, and, in particular, does not depend on the reduced VPF following the negative binomial model. Our result that all galaxy populations studied here have consistent reduced VPFs immediately implies that the VPF can be entirely de-

scribed by $\bar{N}\bar{\xi}$. This, in turn, implies that the VPF is currently incapable of uniquely providing constraints on either cosmological parameters or particular aspects of the halo model, as any useful information provided by the VPF is likewise provided by two-point correlation function analyses; the VPF is of little use in understanding the large scale structure of the universe.

We would like to thank Andreas Berlind, Michael Blanton, Darren Croton, Ofer Lahav, Chung-Pei Ma, Roman Scoccimarro, and Simon White for useful discussions. This project was supported in part by the NSF grants AST00-71198 and AST00-71048. The DEIMOS spectrograph was funded by a grant from CARA (Keck Observatory), an NSF Facilities and Infrastructure grant (AST92-2540), the Center for Particle Astrophysics, and gifts from Sun Microsystems and the Quantum Corporation. C.C. acknowledges support from an NSF REU grant. J.N. acknowledges support from NASA through Hubble Fellowship grant HST-HF-01165.01-A awarded by the Space Telescope Science Institute, which is operated by the Association of Universities for Research in Astronomy, Inc., for NASA, under contract NAS 5-26555. Some of the data presented herein were obtained at the W.M. Keck Observatory, which is operated as a scientific partnership among the California Institute of Technology, the University of California, and the National Aeronautics and Space Administration. The Observatory was made possible by the generous financial support of the W.M. Keck Foundation. In addition, we wish to acknowledge the significant cultural role that the summit of Mauna Kea plays within the indigenous Hawaiian community; we are fortunate to have the opportunity to conduct observations from this mountain.

Funding for the creation and distribution of the SDSS Archive has been provided by the Alfred P. Sloan Foundation, the Participating Institutions, the National Aeronautics and Space Administration, the National Science Foundation, the U.S. Department of Energy, the Japanese Monbukagakusho, and the Max Planck Society. The SDSS Web site is <http://www.sdss.org/>.

The SDSS is managed by the Astrophysical Research Consortium (ARC) for the Participating Institutions. The Participating Institutions are the University of Chicago, Fermilab, the Institute for Advanced Study, the Japan Participation Group, Johns Hopkins University, the Korean Scientist Group, Los Alamos National Laboratory, the Max-Planck-Institute for Astronomy (MPIA), the Max-Planck-Institute for Astrophysics (MPA), New Mexico State University, the University of Pittsburgh, the University of Portsmouth, Princeton University, the United States Naval Observatory, and the University of Washington.

REFERENCES

- Abazajian, K., et al. 2004, *AJ*, 128, 502–512
 Aikio, J., & Maehoenen, P. 1998, *ApJ*, 497, 534
 Antonuccio-Delogu, V., et al. 2002, *MNRAS*, 332, 7–20
 Balian, R., & Schaeffer, R. 1989, *A&A*, 220, 1–2
 Bardeen, J. M., Bond, J. R., Kaiser, N., & Szalay, A. S. 1986, *ApJ*, 304, 15–61
 Baugh, C. M., et al. 2004, *MNRAS*, 351, L44–L48
 Benson, A. J., Hoyle, F., Torres, F., & Vogeley, M. S. 2003, *MNRAS*, 340, 160–174
 Berlind, A. A., & Weinberg, D. H. 2002, *ApJ*, 575, 587–616
 Bernardeau, F., et al. 2002, *Phys. Rep.*, 367, 1–3
 Blanton, M. R., et al. 2003a, *AJ*, 125, 2276–2286
 Blanton, M. R., et al. 2003b, *AJ*, 125, 2348–2360
 Blanton, M. R., et al. 2005, *AJ*, 129, 2562–2578
 Carruthers, P., & Duong-van, M. 1983, *Physics Letters B*, 131, 116–120
 Carruthers, P., & Shih, C. C. 1983, *Physics Letters B*, 127, 242–250
 Coil, A. L., et al. 2004a, *ApJ*, 617, 765–781

- Coil, A. L., et al. 2004b, *ApJ*, 609, 525–538
- Coil, A. L., et al. 2005, *ApJ*, astro-ph/0507647
- Colberg, J. M., Sheth, R. K., Diaferio, A., Gao, L., & Yoshida, N. 2005, *MNRAS*, 360, 216–226
- Cole, S., & Kaiser, N. 1989, *MNRAS*, 237, 1127–1146
- Cooray, A., & Sheth, R. 2002, *Phys. Rep.*, 372, 1–129
- Croton, D. J., et al. 2004, *MNRAS*, 352, 828–836
- Davis, M., et al. 2004, In "Observing Dark Energy", Sidney Wolf and Tod Lauer, editors, ASP Conference Series. [astro-ph/0408344]
- Davis, M., & Geller, M. J. 1976, *ApJ*, 208, 13–19
- Efstathiou, G., Frenk, C. S., White, S. D. M., & Davis, M. 1988, *MNRAS*, 235, 715–748
- Eisenstein, D. J., et al. 2005, *ApJ*, 619, 178–192
- El-Ad, H., & Piran, T. 1997, *ApJ*, 491, 421
- El-Ad, H., Piran, T., & da Costa, L. N. 1996, *ApJ*, 462, L13
- El-Ad, H., Piran, T., & Dacosta, L. N. 1997, *MNRAS*, 287, 790–798
- Elizalde, E., & Gaztanaga, E. 1992, *MNRAS*, 254, 247–256
- Fry, J. N. 1984, *ApJ*, 277, L5–L8
- Fry, J. N. 1985, *ApJ*, 289, 10–17
- Fry, J. N. 1986, *ApJ*, 306, 358–365
- Fry, J. N. 1988, *PASP*, 100, 1336–1339
- Fry, J. N., et al. 1989, *ApJ*, 340, 11–22
- Gaztanaga, E. 1992, *ApJ*, 398, L17–L20
- Gaztanaga, E., et al. 1995, *MNRAS*, 276, 336
- Gaztanaga, E., & Yokoyama, J. 1993, *ApJ*, 403, 450–465
- Ghigna, S., et al. 1994, *ApJ*, 437, L71–L74
- Ghigna, S., Bonometto, S. A., Retzlaff, J., Gottloeber, S., & Murante, G. 1996, *ApJ*, 469, 40
- Goldberg, D. M., & Vogeley, M. S. 2004, *ApJ*, 605, 1–6
- Gott, J. R. I., et al. 2005, *ApJ*, 624, 463–484
- Gottlöber, S., et al. 2003, *MNRAS*, 344, 715–724
- Grogin, N. A., & Geller, M. J. 1999, *AJ*, 118, 2561–2580
- Grogin, N. A., & Geller, M. J. 2000, *AJ*, 119, 32–43
- Hamilton, A. J. S., et al. 1985, *ApJ*, 297, 37–48
- Hamilton, A. J. S., & Tegmark, M. 2004, *MNRAS*, 349, 115–128
- Hoyle, F., et al. 2005, *ApJ*, 620, 618–628
- Hoyle, F., & Vogeley, M. S. 2002, *ApJ*, 566, 641–651
- Hoyle, F., & Vogeley, M. S. 2004, *ApJ*, 607, 751–764
- Kaiser, N. 1984, *ApJ*, 284, L9–L12
- Kaiser, N. 1987, *MNRAS*, 227, 1–21
- Kauffmann, G., & Fairall, A. P. 1991, *MNRAS*, 248, 313–324
- Kauffmann, G., & Melott, A. L. 1992, *ApJ*, 393, 415–430
- Kauffmann, G., Nusser, A., & Steinmetz, M. 1997, *MNRAS*, 286, 795–811
- Kravtsov, A. V., et al. 2004, *ApJ*, 609, 35–49
- Lahav, O., et al. 1993, *ApJ*, 402, 387–397
- Landy, S. D., & Szalay, A. S. 1993, *ApJ*, 412, 64–71
- Little, B., & Weinberg, D. H. 1994, *MNRAS*, 267, 605
- Loveday, J., Maddox, S. J., Efstathiou, G., & Peterson, B. A. 1995, *ApJ*, 442, 457–468
- Müller, V., Arbabi-Bidgoli, S., Einasto, J., & Tucker, D. 2000, *MNRAS*, 318, 280–288
- Ma, C., & Fry, J. N. 2000, *ApJ*, 543, 503–513
- Madgwick, D. S., et al. 2003, *MNRAS*, 344, 847–856
- Mathis, H., & White, S. D. M. 2002, *MNRAS*, 337, 1193–1206
- Maurogordato, S., & Lachieze-Rey, M. 1987, *ApJ*, 320, 13–25
- Mo, H. J., & Boerner, G. 1990, *A&A*, 238, 3–14
- Mo, H. J., & White, S. D. M. 1996, *MNRAS*, 282, 347–361
- Newman, J. A., et al. 2005, *ApJ*, in preparation
- Otto, S., et al. 1986, *ApJ*, 304, 62–74
- Patiri, S. G., et al. 2004, astro-ph/0407513
- Patiri, S. G., Betancort-Rijo, J., Prada, F., Klypin, A., & Gottlöber, S. 2005, ArXiv Astrophysics e-prints
- Peacock, J. A., & Smith, R. E. 2000, *MNRAS*, 318, 1144–1156
- Peebles, P. J. E. 2001, *ApJ*, 557, 495–504
- Rojas, R. R., et al. 2005, *ApJ*, 624, 571–585
- Rojas, R. R., Vogeley, M. S., Hoyle, F., & Brinkmann, J. 2004, *ApJ*, 617, 50–63
- Rood, H. J. 1988, *ARA&A*, 26, 245–294
- Ryden, B. S., & Melott, A. L. 1996, *ApJ*, 470, 160
- Saslaw, W. C., & Hamilton, A. J. S. 1984, *ApJ*, 276, 13–25
- Schmidt, J. D., Ryden, B. S., & Melott, A. L. 2001, *ApJ*, 546, 609–619
- Scoccimarro, R. 2004, *Phys. Rev. D*, 70, 083007
- Seljak, U. 2000, *MNRAS*, 318, 203–213
- Seljak, U. 2001, *MNRAS*, 325, 1359–1364
- Shandarin, S. F., Sheth, J. V., & Sahni, V. 2004, *MNRAS*, 353, 162–178
- Sheth, J. V., et al. 2003, *MNRAS*, 343, 22–46
- Sheth, R. K. 1995, *MNRAS*, 274, 213–220
- Sheth, R. K. 1996, *MNRAS*, 278, 101–110
- Sheth, R. K. 1998, *MNRAS*, 300, 1057–1070
- Sheth, R. K., & van de Weygaert, R. 2004, *MNRAS*, 350, 517–538
- Strauss, M. A., et al. 2002, *AJ*, 124, 1810–1824
- Szapudi, I. 1998, *ApJ*, 497, 16
- Tegmark, M., et al. 2004, *ApJ*, 606, 702–740
- Verde, L., et al. 2002, *MNRAS*, 335, 432–440
- Vogeley, M. S., Geller, M. J., & Huchra, J. P. 1991, *ApJ*, 382, 44–54
- Vogeley, M. S., Geller, M. J., Park, C., & Huchra, J. P. 1994, *AJ*, 108, 745–758
- Weinberg, D. H., & Cole, S. 1992, *MNRAS*, 259, 652–694
- White, M. 2001, *MNRAS*, 321, 1–3
- White, M. 2002, *ApJS*, 143, 241–255
- White, S. D. M. 1979, *MNRAS*, 186, 145–154
- Willmer, C. N. A., et al. 2005, astro-ph/0506041
- Wolf, C., et al. 2003, *A&A*, 401, 73–98
- Yan, R., Madgwick, D. S., & White, M. 2003, *ApJ*, 598, 848–857
- Yan, R., White, M., & Coil, A. L. 2004, *ApJ*, 607, 739–750
- Yang, X., et al. 2003, *MNRAS*, 339, 1057–1080
- York, D. G., et al. 2000, *AJ*, 120, 1579–1587
- Zehavi, I., et al. 2002, *ApJ*, 571, 172–190
- Zehavi, I., et al. 2005a, *ApJ*, 621, 22–31
- Zehavi, I., et al. 2005b, *ApJ*, 630, 1–27